Theoretical model for Rashba spin-orbit interaction in *d* electrons

K. V. Shanavas,* Z. S. Popović,† and S. Satpathy
Department of Physics, University of Missouri, Columbia, Missouri 65221, USA
(Received 17 August 2014; revised manuscript received 23 September 2014; published 7 October 2014)

We show that the Rashba spin-orbit interaction in *d* electron solids, which originates from the broken inversion symmetry at surfaces or interfaces, is strongly dependent on the orbital characters of the bands involved. This is studied by developing a tight-binding model in the presence of a uniform perpendicular electric field and spin-orbit coupling. We argue that for valence electrons, the spin-orbit coupling strength scales only as the square of the atomic number. The electric field distorts the *d* orbitals through the admixture of *p* and *f* states and also introduces intersite overlap parameters. Expressions for Rashba coefficients for the bands are obtained in both weak and strong spin-orbit interaction limits and are shown to be orbital dependent. The results are compared with first-principles calculations for model systems, showing good agreement. Our study demonstrates the orbital-dependent gate control of the Rashba effect for the purposes of oxide electronics.

DOI: 10.1103/PhysRevB.90.165108 PACS number(s): 73.20.−r, 71.10.−w, 31.15.A−

I. INTRODUCTION

The recent discovery of the Rashba effect [1] in the two-dimensional electron gas (2DEG) systems such as perovskite surfaces and interfaces has led to the possibility of tuning its properties by external electric fields [2]. The study of the Rashba effect in 2DEGs is of interest not just from a fundamental point of view, but also due to potential applications in spintronics devices [3]. In contrast to their semiconductor counterparts, the perovskites are characterized by the presence of high-*Z* elements and *d* electrons with strong spin-orbit interaction.

For 2D electrons confined to the xy plane and subjected to an electric field along $\hat{z}$, the Rashba splitting is commonly described by the Bychkov-Rashba Hamiltonian [4],

$$\mathcal{H}_R = \alpha_R(\vec{\sigma} \times \vec{k}) \cdot \hat{z} = \alpha_R(k_y\sigma_x - k_x\sigma_y), \qquad (1)$$

where $\vec{k} = (k_x,k_y,0)$ is the electron crystal momentum, $\vec{\sigma} = (\sigma_x,\sigma_y,\sigma_z)$ are the Pauli matrices, and α_R is the Rashba coefficient. The Rashba effect originates from a combination of the inversion symmetry breaking and spin-orbit interaction and has predominant contribution from the nuclear regions in the solid [5,6]. It has been observed in numerous condensed-matter systems including metal surfaces [7,8], topological insulators [9,10], interfaces of perovskite oxides [2,11–13], etc.

On the theoretical side, tight-binding (TB)-based model Hamiltonian approaches [14,15] have been successful in understanding the Rashba effect in solids. The basic idea is to incorporate the effect of broken inversion symmetry phenomenologically into atomic orbital overlap parameters. For example, in the case of *p* orbitals on a plane, the coupling between in-plane p_x, p_y orbitals and out-of-plane p_z orbitals is zero. However, if the symmetry is broken by an external field, it leads to matrix elements between these orbitals [14] and, in conjunction with spin-orbit interaction, will result in effective couplings between spin-up and spin-down bands.

These ideas have been used to study the Rashba effect in several systems of current interest such as graphene [16–18] and polar complex oxides [6,19–21]. In the case of graphene, which is a sp-band system, model studies showed that in addition to the intersite coupling terms similar to the one proposed earlier, there also exist on-site terms that play an important role [18]. They arise from electric-field-induced couplings with orbitals that satisfy the selections rules $\Delta l = \pm 1$ and $\Delta m = 0$ at the same site, as these atomic wave functions are no longer orthogonal in the presence of external electric field.

At the complex oxides interfaces of $LaAlO_3/SrTiO_3$ and surfaces of $KTaO_3$, a 2DEG with transition-metal (Ti or Ta) *d* orbital character develops. These systems have strong spin-orbit interaction and the structural inversion symmetry is broken at the interfaces/surfaces, making them good candidates for exhibiting a strong Rashba effect. In the case of the $LaAlO_3/SrTiO_3$ interface, it was shown that the magnitude of the splitting can be tuned by an applied gate voltage [2]. Tight-binding models [19,21] for the t_{2g} states on a cubic lattice were found to agree well with first-principles calculations based on the density functional theory (DFT). It has also been suggested that the polar distortions of the metal ion oxygen bonds also play an important role in Rashba splitting [20]. From density functional calculations of $KTaO_3$, we showed earlier that the 2DEG can be manipulated by the electric field to go in and out of the surface, offering a method to tailor the magnitude of the Rashba splitting [6].

In this paper, we present detailed theoretical models to understand the dependence of the Rashba coefficient on the orbital character and spin-orbit (SO) coupling of the atomic states in the material. We obtain expressions for α_R in the weak and strong SO interaction limits. First-principles calculations are performed on model systems containing a single atomic layer of Ti or Ta on a square lattice, to make connection with the TB model.

This paper is organized as follows. In the next section, we discuss the orbital dependence of spin-orbit coupling strength, which is a crucial ingredient in the Rashba effect in solids. In Sec. III, we construct the tight-binding Hamiltonian for *d* orbitals under a uniform electrostatic potential and discuss the origin of various contributions. The derivation of effective

*Present address: Oak Ridge National Laboratory, 1 Bethel Valley Road, Oak Ridge, Tennessee 37831, USA; kavungalvees@ornl.gov
†Permanent address: Institute of Nuclear Sciences, Vinča, University of Belgrade, P. O. Box 522, 11001 Belgrade, Serbia.

Hamiltonians for individual bands is discussed in Sec. IV. Finally, the results from the tight-binding model are compared with first-principles calculations in Sec. V.

II. VARIATION OF SPIN-ORBIT COUPLING WITH ATOMIC NUMBER

It is well known that the spin-orbit interaction strength λ increases rapidly with the atomic number Z. However, there is some confusion in the literature regarding just how rapid this increase is. We clarify this issue here and emphasize that the spin-orbit interaction strength for the *outer* electrons in the atom, i.e., the electrons that are relevant to the properties in the solid state, increases only as the Landau-Lifshitz scaling Z^2, while it increases much more rapidly within a certain series such as $3d$, where it scales as Z^4 as suggested by the simple hydrogenic result. The Landau-Lifshitz scaling argument [22] is based on an estimate of the penetration of the outer electrons, rather than the electrons of a particular series, into the nuclear region where the bulk of the spin-orbit interaction originates.

The origin of the Z^4 dependence is well known. The spin-orbit interaction of an electron in a central field of potential $V(r)$ is given by the expression

$$\mathcal{H}_{\rm SO}(r) = \frac{r^{-1}}{2m^2c^2}\frac{\partial V(r)}{\partial r}\vec{L}\cdot\vec{S} = \lambda(r)\vec{L}\cdot\vec{S}, \qquad (2)$$

and if we evaluate its expectation value using the Coulomb potential $V(r) = -Ze^2/r$ and the hydrogenic wave functions $R_{nl}(r)$ with energy E^0_{nl}, we get the well-known result for the perturbative correction due to the spin-orbit interaction, viz. [23],

$$E_{nl} = E^0_{nl} + \lambda_{nl} \times 2^{-1}[j(j+1) - l(l+1) - 3/4], \qquad (3)$$

where j and l are total and orbital angular momentum quantum numbers with

$$\lambda_{nl} = \int_0^\infty R^2_{nl}\lambda(r)d^3r = \frac{\alpha^2 Z^4}{n^3 l(l+1/2)(l+1)}\ {\rm Ry}, \qquad (4)$$

which increases as Z^4, with α being the fine-structure constant. To see how well this is obeyed in the actual atoms, we have taken the spin-orbit interaction strength λ_{nl}, calculated by Herman and Skillman [24] using the Hartree-Fock method with the Slater exchange, and have plotted these in Fig. 1 along with the hydrogenic expression given by Eq. (4) for the $3d$ series. As seen from the figure, even though the Z^4 power dependence is not too bad for large Z for a particular series, the magnitude of λ_{nl} is nevertheless severely overestimated by Eq. (4). This is not surprising because the hydrogenic result neglected the screening of the nuclear potential by the innermost core electrons.

However, in the solid, the outer electrons are the relevant electrons, whose quantum numbers nl change with Z. If one considers the outermost electrons for the atoms without worrying about nl, then Landau and Lifshitz have argued that the spin-orbit interaction strength should scale more like Z^2, viz.,

$$\lambda = A\alpha^2 Z^2\ {\rm Ry}, \qquad (5)$$

where A is of the order of one. We find that if we consider the *outer* electrons in the atom (shown by dots and the shaded area in Fig. 1), then λ_{nl} does roughly follow this Z^2 dependence with $A \approx 0.1$, as illustrated in Fig. 1. Note that the Z^2 dependence describes the rough overall systematic variation of the spin-orbit interaction strength and not the nonsystematic change from element to element. Thus the strength of the relevant spin-orbit interaction, viz., that for the *outer* electrons, does not increase nearly as fast as Z^4 as sometimes thought in the literature based on the hydrogenic expression given by Eq. (4). The spin-orbit interaction strengths for the atoms considered in this paper are listed in Table I.

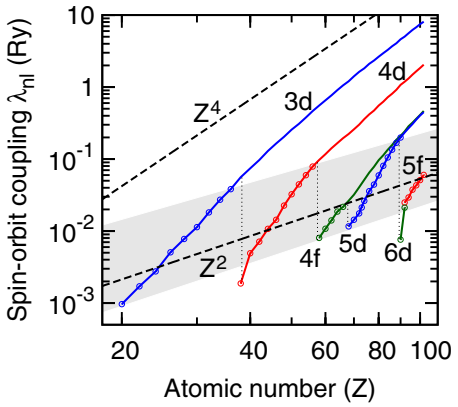

FIG. 1. (Color online) Dependence of the spin-orbit coupling strength λ_{nl} for atoms as a function of the atomic number Z. The calculated results of Herman and Skillman [24] using the Hartree-Fock method (colored lines) are compared to the hydrogenic Z^4 dependence, which is computed from Eq. (4) for the $3d$ series (upper dashed line). For the *outermost* electrons (indicated by the circles and the shaded area), which are the relevant electrons in the solid, the quantum numbers nl change with Z and the spin-orbit interaction increases much more slowly, following roughly the Landau-Lifshitz Z^2 scaling [lower dashed line, calculated from Eq. (5) with $A = 0.10$].

III. TIGHT-BINDING MODEL

To describe the Rashba spin-orbit interaction, the model Hamiltonian should have three terms: a band structure term $\mathcal{H}_{\rm K}$, a spin-orbit term $\mathcal{H}_{\rm SO}$, and the electric-field-induced inversion symmetry-breaking term $\mathcal{H}_{\rm E}$,

$$\mathcal{H} = \mathcal{H}_{\rm K} + \mathcal{H}_{\rm SO} + \mathcal{H}_{\rm E}. \qquad (6)$$

TABLE I. Spin-orbit coupling strength (in eV) for the outermost electrons in the atoms considered in this work as obtained from the hydrogenic expression [$\lambda_{\rm Hyd}$, Eq. (4)], the Landau-Lifshitz scaling [$\lambda_{\rm LL}$, Eq. (5)], and the Hartree-Fock calculations of Herman and Skillman ($\lambda_{\rm HF}$). The last column $\lambda_{\rm solid}$ lists the calculated values for the solid from the present DFT calculations. The atomic values differ from $\lambda_{\rm solid}$ because of the admixture of other orbitals and the delocalized nature of the outermost electrons in the solid as compared to the atom.

Element	Z	$\lambda_{\rm Hyd}$	$\lambda_{\rm LL}$	$\lambda_{\rm HF}$	$\lambda_{\rm solid}$
Ti 3d	22	0.42	0.035	0.023	0.02
Ta 5d	73	11	0.39	0.30	0.18

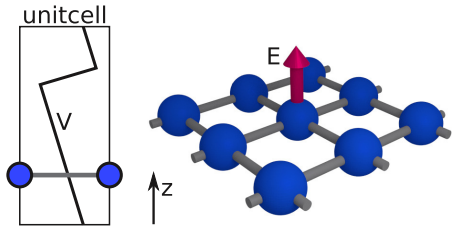

FIG. 2. (Color online) The model contains a square lattice with an applied electric field along the $\hat{z}$ direction (right). First-principles calculations in Sec. V are carried out on a unit cell with ∼10 Å vacuum and a sawtooth potential (left).

To model the 2DEG at the perovskite structures, we would like to use a linear combination of atomic d orbitals as basis functions denoted by $|\phi_{\alpha\vec{R}}\rangle$, where α is the combined orbital and spin index and $\vec{R}$ is the lattice vector, which points to atoms on a square lattice, as shown in Fig. 2. Note that in actual systems, the d orbitals are interconnected through oxygen p states. Since spin-orbit interaction (SOI) in oxygen is quite small, we can incorporate their effect as an effective d-d coupling.

The electrostatic potential $\mathcal{H}_{\rm E}$ breaks the spherical symmetry around the atoms and distorts the atomic orbitals. But it is much weaker than the nuclear potential, hence, we can treat $\mathcal{H}_{\rm E}$ as a perturbation and write

$$\mathcal{H} = \mathcal{H}_0 + \zeta\mathcal{H}_{\rm E}, \tag{7}$$

where $\mathcal{H}_0 = \mathcal{H}_{\rm K} + \mathcal{H}_{\rm SO}$ and ζ is a dimensionless parameter ($\zeta = 1$). With $|\phi^1_{\alpha\vec{R}}\rangle$ as the first-order corrections to the atomic orbitals, we can write the matrix elements of $\mathcal{H}$ as

$$\begin{aligned}
&\langle\phi_{\alpha\vec{0}} + \zeta\phi^1_{\alpha\vec{0}}|\mathcal{H}_0 + \zeta\mathcal{H}_{\rm E}|\phi_{\beta\vec{R}} + \zeta\phi^1_{\beta\vec{R}}\rangle \\
&\quad= \langle\phi_{\alpha\vec{0}}|\mathcal{H}_{\rm K}|\phi_{\beta\vec{R}}\rangle + \langle\phi_{\alpha\vec{0}}|\mathcal{H}_{\rm SO}|\phi_{\beta\vec{R}}\rangle + \zeta\langle\phi_{\alpha\vec{0}}|\mathcal{H}_{\rm E}|\phi_{\beta\vec{R}}\rangle \\
&\qquad+ \zeta\left[\langle\phi_{\alpha\vec{0}}|\mathcal{H}_0|\phi^1_{\beta\vec{R}}\rangle + \langle\phi^1_{\alpha\vec{0}}|\mathcal{H}_0|\phi_{\beta\vec{R}}\rangle\right] + O(\zeta^2) \\
&\quad= T_{\rm K} + T_{\rm SO} + T_{\rm E} + T_1,
\end{aligned} \tag{8}$$

where $T_{\rm K}, T_{\rm SO}$, and $T_{\rm E}$ are matrix elements with the unperturbed orbitals and T_1 are the matrix elements introduced by the perturbation. We ignore terms quadratic in ζ. Note that we have taken into account the fact that not only does the changed Hamiltonian modify the hopping integral between the original basis orbitals, but in addition the basis orbitals themselves become modified via the admixture of other atomic orbitals at the same site, viz., the p and the f orbitals. In other words, the Hilbert space axes become modified as well. We discuss the individual terms in detail below.

A. Kinetic-energy terms $T_{\rm K}$

The periodic nature of the lattice helps us construct the matrix elements $\langle\phi_{\alpha\vec{0}}|\mathcal{H}_{\rm K}|\phi_{\beta\vec{R}}\rangle$ in the reciprocal space by writing the atomic orbitals as a Bloch sum,

$$|\chi_{\alpha\vec{k}}\rangle = \frac{1}{\sqrt{N}}\sum_{\vec{R}} e^{i\vec{k}\cdot\vec{R}}|\phi_{\alpha\vec{R}}\rangle. \tag{9}$$

Therefore,

$$T_{\rm K}(\vec{k}) = \varepsilon_\alpha\delta_{\alpha\beta} + \sum_{\langle\vec{R}\rangle} e^{i\vec{k}\cdot\vec{R}}T_{\rm K}(\vec{R}). \tag{10}$$

The sum runs over the nearest-neighbor lattice sites except the central site, $\vec{R} = 0$, which produces the first term, with ε_α being the on-site energies. For the atomic orbitals in the order $\phi_\alpha \equiv \{d_{z^2}, d_{x^2-y^2}, d_{xy}, d_{xz}, d_{yz}\}$, the $\hat{T}_{\rm K}$ matrix can be written with the help of Slater-Koster tables [25,26],

$$\hat{T}_{\rm K} = \begin{pmatrix} h_1 & h_{12} & 0 & 0 & 0 \\ h_{12}^* & h_2 & 0 & 0 & 0 \\ 0 & 0 & h_3 & 0 & 0 \\ 0 & 0 & 0 & h_4 & 0 \\ 0 & 0 & 0 & 0 & h_5 \end{pmatrix}, \tag{11}$$

where

$$\begin{aligned}
h_1 &= \varepsilon_1 + (V_\sigma/2 + 3V_\delta/2)(\cos k_x a + \cos k_y a), \\
h_2 &= \varepsilon_2 + (3V_\sigma/2 + V_\delta/2)(\cos k_x a + \cos k_y a), \\
h_{12} &= (\sqrt{3}V_\delta/2 - \sqrt{3}V_\sigma/2)(\cos k_x a - \cos k_y a), \\
h_3 &= \varepsilon_3 + 2V_\pi(\cos k_x a + \cos k_y a), \\
h_4 &= \varepsilon_4 + 2(V_\pi\cos k_x a + V_\delta\cos k_y a), \\
h_5 &= \varepsilon_5 + 2(V_\pi\cos k_y a + V_\delta\cos k_x a),
\end{aligned} \tag{12}$$

V_σ, V_π, and V_δ are the Slater-Koster parameters for d-d overlap, ε_i are the on-site energies, and a is the nearest-neighbor distance.

B. Spin-orbit terms $T_{\rm SO}$

From Eq. (2), we can construct matrix elements of SOI for d states,

$$\hat{T}_{\rm SO} = \frac{i\lambda}{2}\begin{pmatrix} 0 & 0 & 0 & -\sqrt{3}\sigma_y & \sqrt{3}\sigma_x \\ 0 & 0 & -2\sigma_z & \sigma_y & \sigma_x \\ 0 & 2\sigma_z & 0 & -\sigma_x & \sigma_y \\ \sqrt{3}\sigma_y & -\sigma_y & \sigma_x & 0 & -\sigma_z \\ -\sqrt{3}\sigma_x & -\sigma_x & -\sigma_y & \sigma_z & 0 \end{pmatrix}, \tag{13}$$

where, $\sigma_x, \sigma_y, \sigma_z$ are the 2×2 Pauli spin matrices. SOI has only on-site terms and no k dependence. To understand the effect of λ on Rashba splitting, we consider two limits. (1) The first limit is a weak SOI, with $\lambda \ll V$, where V is the electron hopping parameter. In the first-principles calculations (Sec. V), this case is simulated using $3d$ ion Ti with $Z = 22$. (2) The second limit is a strong SOI, with $\lambda \gg V$, which is simulated by the $5d$ element Ta with $Z = 73$. The values of λ obtained for these two cases using the methods discussed above are summarized in Table I.

C. Perturbative terms T_1

To evaluate the matrix elements T_1, we first write down the expression for the first-order correction from perturbation theory,

$$|\phi^1_{\alpha\vec{R}}\rangle = \sum_{\beta\neq\alpha}\frac{\langle\phi_{\beta\vec{R}}|\mathcal{H}_{\rm E}|\phi_{\alpha\vec{R}}\rangle}{\epsilon_\alpha - \epsilon_\beta}|\phi_{\beta\vec{R}}\rangle, \tag{14}$$

where the index α runs over the five d orbitals of interest here, and β runs over all other atomic orbitals at the same site. The perturbation $\mathcal{H}_{\rm E}$ may originate from an external electric field or proximity of an atom to a surface, which also breaks the inversion symmetry. In the simplest form, it can be written in terms of the effective electric field η,

$$\mathcal{H}_{\rm E} = \eta z, \tag{15}$$

which may be different from the applied electric field due to electronic and ionic screening [6].

Now, we can write $\phi_{\alpha\vec{R}} = R_\alpha(|\vec{r}-\vec{R}|)\tilde{Y}_\alpha(\theta,\phi)$ and $z = (4\pi/3)^{1/2}\, rY_{10}$. The cubic harmonics $\tilde{Y}_\alpha$ can be expressed in terms of the spherical harmonics Y_{lm}, so the matrix elements in Eq. (14) boil down to a product of an integral over r and an angular integral over the product of three spherical harmonics. The angular part of the integral can be solved with the help of the Gaunt coefficients $C_{lm,l'm',l''m''}$ defined as [27,28]

$$\begin{aligned} C_{lm,l'm',l''m''} &= \int \mathrm{Y}_{lm}(\theta,\phi)\mathrm{Y}^*_{l'm'}(\theta,\phi)\mathrm{Y}_{l''m''}(\theta,\phi)\, d\Omega \\ &= \left(\frac{2l''+1}{4\pi}\right)^{1/2} c^{l''}(l'm';lm). \end{aligned} \tag{16}$$

The coefficients $c^{l''}(l'm';lm)$ vanish unless $m'' = m'-m$ and $l'' = |l-l'|, |l-l'|+2, \ldots, (l+l')$ [23]. The second condition couples the d orbitals only to the p and the f orbitals ($\Delta l = \pm 1$) and the first condition requires $\Delta m = m''-m' = 0$.

Following the above procedure to evaluate Eq. (14), we find that the first-order correction to the d orbitals contains just a few terms, viz.,

$$\begin{aligned} |d^1_{z^2}\rangle &= \frac{2\eta_{\rm p}}{\sqrt{15}}|p_z\rangle + \frac{3\eta_{\rm f}}{\sqrt{35}}|f_{z^3}\rangle, \\ |d^1_{x^2-y^2}\rangle &= \frac{\eta_{\rm f}}{\sqrt{7}}|f_{zx^2-zy^2}\rangle, \\ |d^1_{xy}\rangle &= \frac{\eta_{\rm f}}{\sqrt{7}}|f_{xyz}\rangle, \\ |d^1_{xz}\rangle &= \frac{\eta_{\rm p}}{\sqrt{5}}|p_x\rangle + \frac{2\sqrt{2}\eta_{\rm f}}{\sqrt{35}}|f_{xz^2}\rangle, \\ |d^1_{yz}\rangle &= \frac{\eta_{\rm p}}{\sqrt{5}}|p_y\rangle + \frac{2\sqrt{2}\eta_{\rm f}}{\sqrt{35}}|f_{yz^2}\rangle, \end{aligned} \tag{17}$$

where

$$\eta_\beta = \frac{\eta}{\varepsilon_d - \varepsilon_\beta}\int dr\, R_\beta(r) r R_d(r),$$

which is a dimensionless parameter that depends on the energy separation and radial spread of the orbitals. Figure 3 shows the asymmetric d_{z^2} orbital because of the admixture with the other orbitals at the same site.

Thus, T_1 includes p-d and d-f hopping parameters due to the admixture of d orbitals with these orbitals. The only contribution towards T_1 comes from $H_{\rm K}$ with $R \neq 0$, since $H_{\rm SO}$ does not couple different angular momentum and since on-site terms of $H_{\rm K}$ between different orbitals are zero. Evaluating all

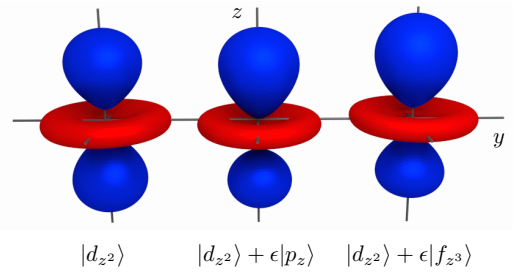

FIG. 3. (Color online) Contour plot of $3d_{z^2}$ orbital showing the effect of the electric-field-induced mixing with the p_z and f_{z^3} orbitals with $\epsilon = 0.3$. The colors differentiate the signs of the wave function.

the matrix elements for nearest neighbors, we get

$$\hat{T}_0 = \begin{pmatrix} 0 & 0 & 0 & h_{14} & h_{15} \\ 0 & 0 & 0 & h_{24} & h_{25} \\ 0 & 0 & 0 & h_{34} & h_{35} \\ h^*_{14} & h^*_{24} & h^*_{34} & 0 & 0 \\ h^*_{15} & h^*_{25} & h^*_{35} & 0 & 0 \end{pmatrix}, \tag{18}$$

where

$$\begin{aligned} h_{14} &= 2i\gamma_1 \sin k_x a, \quad h_{15} = 2i\gamma_1 \sin k_y a, \\ h_{24} &= 2i\gamma_2 \sin k_x a, \quad h_{25} = -2i\gamma_2 \sin k_y a, \\ h_{34} &= 2i\gamma_3 \sin k_y a, \quad h_{35} = 2i\gamma_3 \sin k_x a, \end{aligned} \tag{19}$$

the electric-field-dependent parameters γ_1, γ_2, and γ_3 are

$$\begin{aligned} \gamma_1 &= \eta_{\rm p}\left[\frac{V_{pd\sigma}}{2\sqrt{5}} + \frac{2V_{pd\pi}}{\sqrt{15}}\right] + \eta_{\rm f}\left[\frac{\sqrt{3}V_{df\sigma}}{2\sqrt{35}} + \frac{3\sqrt{3}V_{df\pi}}{2\sqrt{70}}\right], \\ \gamma_2 &= -\frac{\sqrt{3}\eta_{\rm p}V_{pd\sigma}}{2\sqrt{5}} - \eta_{\rm f}\left[\frac{3V_{df\sigma}}{2\sqrt{35}} + \frac{\sqrt{5}V_{df\pi}}{2\sqrt{14}}\right], \\ \gamma_3 &= -\frac{\eta_{\rm p}V_{pd\pi}}{\sqrt{5}} - \frac{\eta_{\rm f}V_{df\pi}}{\sqrt{70}}, \end{aligned} \tag{20}$$

and $V_{pd\sigma}$ ($V_{df\sigma}$) and $V_{pd\pi}$ ($V_{df\pi}$) are σ and π hopping between p (f) and d orbitals on neighboring sites. We can make an approximate estimate of the parameters γ by using the analytical expressions for p-d hopping [26],

$$V_{pd(\sigma/\pi)} = n_{pd(\sigma/\pi)}\frac{\hbar^2 r_a^{3/2}}{m a^{7/2}}, \tag{21}$$

where a is the nearest-neighbor distance. For typical values of p-d hopping parameters, $n_{pd\sigma} = -3.14$, $\eta_{pd\pi} = 1.36$, $\hbar^2/m = 7.62$ eV Å^2, and $r_a = 1.08$ Å. Variations of the γ's as a function of neighbor distance are shown in Fig. 4. Close to the origin, γ_2 and γ_3 diverge and the empirical expressions for hopping given in Eq. (21) are valid only for larger distances. Due to symmetry, the two terms involving $V_{dp\sigma}$ and $V_{dp\pi}$ in the expression for γ_1 cancel each other exactly.

D. Electrostatic potential terms $T_{\rm E}$

The matrix elements $T_{\rm E} = \langle\phi_{\alpha\vec{0}}|\eta z|\phi_{\beta\vec{R}}\rangle$ represent coupling between d orbitals on different sites due to the electrostatic potential. The integral is too complicated to solve analytically, so we evaluate it numerically assuming hydrogenic functions

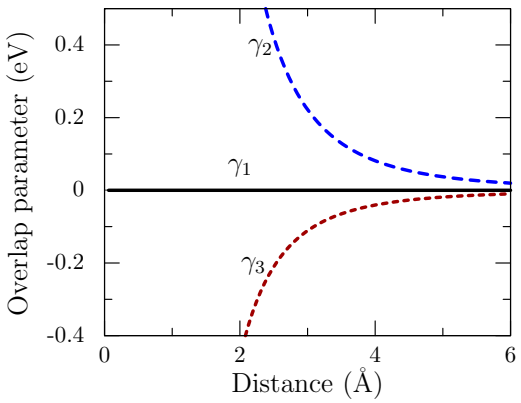

FIG. 4. (Color online) Electric-field-induced overlap parameters due to the perturbative term T_1 as a function of the nearest-neighbor distance, calculated from Eqs. (20) and (21) using typical values for the parameters $\eta_{pd\sigma} = -3.14$, $\eta_{pd\pi} = 1.36$, $r_a = 1.08$ Å, $\eta_p = 1$, and $\eta_f = 0$.

with a screened nuclear charge Z_e for the radial part of the wave functions,

$$R_\alpha(r) = \sqrt{\left(\frac{2Z_e}{na_0}\right)^3 \frac{(n-l-1)!}{2n(n+l)!}} e^\rho \rho^l L^{2l+1}_{n-l-1}(\rho), \qquad (22)$$

where $\rho = (2Z_e/na_0)r$, a_0 is the Bohr radius, and $L(\rho)$ is the associated Laguerre polynomials. We find that there are three nonzero coupling parameters, viz.,

$$\begin{aligned}
\gamma_1' &= \eta\langle d_{z^2}|z|d_{xz},a\hat{x}\rangle = \eta\langle d_{z^2}|z|d_{yz},a\hat{y}\rangle,\\
\gamma_2' &= \eta\langle d_{x^2-y^2}|z|d_{xz},a\hat{x}\rangle = \eta\langle d_{yz}|z|d_{x^2-y^2},a\hat{y}\rangle, \qquad (23)\\
\gamma_3' &= \eta\langle d_{xy}|z|d_{xz},a\hat{y}\rangle = \eta\langle d_{xy}|z|d_{yz},a\hat{x}\rangle.
\end{aligned}$$

Here, the orbital on the left side of the inner product is at the origin, while the one on the right is located on a neighboring atom shifted by the lattice constant a along the indicated direction.

The coupling parameters, shown in Fig. 5, become negligible for distances beyond 5 Å. For a typical $3d$ element such as Ti, the covalent radius is about 1.5 Å, so d-d distances are

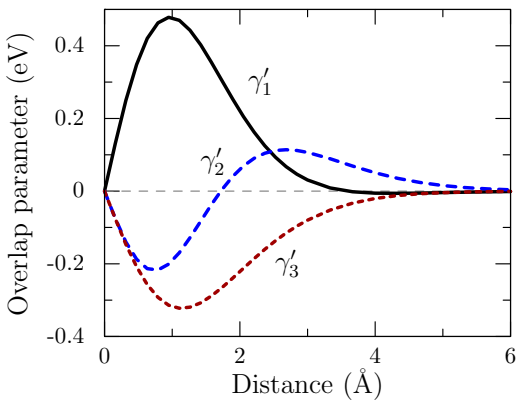

FIG. 5. (Color online) Electric-field-induced overlap parameters due to the intersite contribution term T_E obtained from Eqs. (22) and (23) and numerical integration for $3d$ wave functions with parameter values $n = 3, l = 2, Z_e = 4$, and $\eta = 1$ eV/Å.

~3 Å. In this range, the strongest contribution comes from γ_2', followed by γ_3' and γ_1', which is understandable since $d_{x^2-y^2}$ and d_{xy} have the largest spread in the xy plane. However, for shorter distances, γ_1' is the largest, as the electric field has the strongest effect on d_{z^2} since it lies along the z axis. Figure 5 shows that the relative magnitudes of the electric-field-induced couplings between orbitals can be tuned by changing the lattice spacing, and therefore also the Rashba effect with applied pressure. In the Bloch function basis, one can write down T_E explicitly in the matrix form just like Eq. (18), and it is seen that it has exactly the same k dependence as T_1, which is a consequence of the same symmetry in both cases. However, they may have different forms for other systems. In the present case, we can use Eq. (18) as the full electric-field contribution by redefining the parameters as

$$\gamma_i \to \gamma_i + \gamma_i'. \qquad (24)$$

Finally, collecting all the terms, viz., Eqs. (11), (13), (18), and (24), the 10×10 TB Hamiltonian in the orbital-spin space can be written as

$$\mathcal{H} = (\hat{T}_K + \hat{T}_1) \otimes \mathbb{1} + \hat{T}_{SO}, \qquad (25)$$

where $\mathbb{1}$ is the identity matrix in the spin-1/2 space. After taking the five on-site energies ε_i to be zero for simplicity, we have seven other TB parameters: $V_\sigma, V_\pi, V_\delta, \lambda, \gamma_1, \gamma_2$, and γ_3. They depend on specific systems, and in Sec. V we discuss typical values derived from DFT calculations on Ti and Ta systems.

IV. EFFECTIVE HAMILTONIAN

By diagonalizing the full Hamiltonian in Eq. (25) at different k points with appropriate parameter values, we can study the energy levels in the system. For the 2DEG in perovskite materials, the important region in the reciprocal space is around the zone center. At the Γ point, the d states are split into five doubly degenerate states by electron hopping and spin-orbit coupling. The levels are spin degenerate when $k = 0$, since the effect of the electric field is zero. As long as the states are well separated, we can describe the effect of momentum-dependent spin splitting around the Γ point for each band by a 2×2 Rashba Hamiltonian. The effect of the remaining eight-dimensional subspace is folded via renormalization of the parameters. To illustrate this, we consider two limits of parameter values, when spin orbit is weak compared to electron coupling, and vice versa. The energy levels at the Γ point in both cases are shown in Fig. 6.

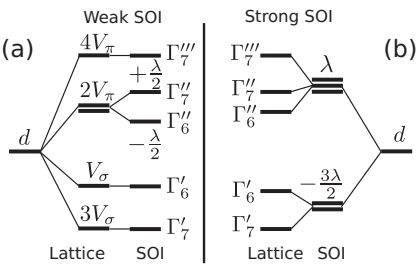

FIG. 6. Energy splitting for a square lattice at the Γ point in the presence of (a) weak and (b) strong spin-orbit interaction compared to the electron hopping parameters V_σ, V_π.

TABLE II. Energy- and orbital-dependent Rashba coefficients in the weak and strong spin-orbit interaction limits. The Rashba coefficients α_R/a (in meV) obtained from the TB expressions are compared with numerical results from the DFT and TB calculations. For simplicity, V_δ is neglected as compared to V_σ and V_π in the TB expressions. DFT calculations are for the square lattice of Ti and Ta for cases of weak and strong SOI, respectively. The TB expressions given here are correct to the lowest order; omitted terms are $O(\lambda^2)$ for the weak SOI case and $O(\gamma/\lambda)$ or $O(\gamma/V)$ for the strong SOI case.

			TB			DFT	
	Sym	Energy at Γ	α_R/a (downfolding)	α_R/a (downfolding)	$\lvert\alpha_R/a\rvert$ (full H)	Orbital character	$\lvert\alpha_R/a\rvert$
Weak SOI ($\lambda \ll V_\sigma, V_\pi$)	Γ_7'	$3V_\sigma$	$2\lambda\gamma_2/(-3V_\sigma + 2V_\pi)$	−0.62	0.73	x^2-y^2	0.69
	Γ_6'	V_σ	$2\sqrt{3}\lambda\gamma_1/(V_\sigma - 2V_\pi)$	−5.64	4.13	z^2	4.13
	Γ_6''	$2V_\pi - \lambda/2$	$-2\sqrt{3}\lambda\gamma_1/(V_\sigma - 2V_\pi)$	5.64	4.25	xz/yz	7.62
	Γ_7''	$2V_\pi + \lambda/2$	$2\lambda\gamma_2/(3V_\sigma - 2V_\pi) + \lambda\gamma_3/V_\pi$	0.93	1.02	xz/yz	1.00
	Γ_7'''	$4V_\pi$	$-\lambda\gamma_3/V_\pi$	−0.57	0.30	xy	0.42
Strong SOI($\lambda \gg V_\sigma, V_\pi$)	Γ_7'	$-3\lambda/2 + 6V_\sigma/5 + 2V_\pi$	$4(\gamma_2 - \gamma_3)/5$	13.60	9.78	x^2-y^2/xy	9.05
	Γ_6'	$-3\lambda/2 + 2V_\sigma/5 + 6V_\pi/5$	$-4\sqrt{3}\gamma_1/5$	−9.00	6.88	$z^2/xz/yz$	6.23
	Γ_7''	$\lambda + 9V_\sigma/5 + 4V_\pi/3$	$-(4/5\gamma_2 + 8/15\gamma_3)$	−14.9	13.2	xy/x^2-$y^2/xz/yz$	10.33
	Γ_6''	$\lambda + 3V_\sigma/5 + 4V_\pi/5$	$4\sqrt{3}\gamma_1/5$	9.00	6.88	$z^2/xz/yz$	11.80
	Γ_7'''	$\lambda + 8V_\pi/3$	$4\gamma_3/3$	1.33	3.50	$xy/xz/yz$	2.63

A. Weak SOI ($\lambda \ll V$)

The energy levels at the Γ point, obtained from the full tight-binding Hamiltonian, are given in Fig. 6(a). Bond formations split the states into four, where d_{xz} and d_{yz} are degenerate due to symmetry. The symmetry is further lifted by SOI. The character of the bands at these energies is given below,

$$\Gamma_7' = \begin{Bmatrix} d_{x^2-y^2\uparrow} \\ d_{x^2-y^2\downarrow} \end{Bmatrix}, \quad \Gamma_7'' = \begin{Bmatrix} \frac{1}{\sqrt{2}}(d_{xz\downarrow} - id_{yz\downarrow}) \\ \frac{1}{\sqrt{2}}(d_{xz\uparrow} + id_{yz\uparrow}) \end{Bmatrix}, \quad \Gamma_7''' = \begin{Bmatrix} d_{xy\uparrow} \\ d_{xy\downarrow} \end{Bmatrix}, \quad \Gamma_6' = \begin{Bmatrix} d_{z^2\uparrow} \\ d_{z^2\downarrow} \end{Bmatrix}, \quad \Gamma_6'' = \begin{Bmatrix} \frac{1}{\sqrt{2}}(d_{xz\downarrow} + id_{yz\downarrow}) \\ \frac{1}{\sqrt{2}}(d_{xz\uparrow} - id_{yz\uparrow}) \end{Bmatrix}. \tag{26}$$

The full Hamiltonian in Eq. (25) can be transformed into the basis set for weak SOI given in Eq. (26) by a unitary transformation $U^\dagger \mathcal{H} U$,

$$\mathcal{H}_U = \begin{pmatrix} \Gamma_7' & & \Gamma_6' & & \Gamma_6'' & & \Gamma_7'' & & \Gamma_7''' & \\ \hline 3V_\sigma & 0 & 0 & 0 & 0 & 0 & \frac{\lambda}{\sqrt{2}} & 0 & -i\lambda & 0 \\ 0 & 3V_\sigma & 0 & 0 & 0 & 0 & 0 & -\frac{\lambda}{\sqrt{2}} & 0 & i\lambda \\ 0 & 0 & V_\sigma & 0 & -\sqrt{\frac{3}{2}}\lambda & k^+\gamma_1 & 0 & -k^-\gamma_1 & 0 & 0 \\ 0 & 0 & 0 & V_\sigma & -k^-\gamma_1 & \sqrt{\frac{3}{2}}\lambda & k^+\gamma_1 & 0 & 0 & 0 \\ 0 & 0 & -\sqrt{\frac{3}{2}}\lambda & -k^+\gamma_1 & -\frac{\lambda}{2} & 0 & 0 & 0 & 0 & 0 \\ 0 & 0 & k^-\gamma_1 & \sqrt{\frac{3}{2}}\lambda & 0 & -\frac{\lambda}{2} & 0 & 0 & 0 & 0 \\ \frac{\lambda}{\sqrt{2}} & 0 & 0 & k^-\gamma_1 & 0 & 0 & \frac{\lambda}{2} & 0 & \frac{i\lambda}{\sqrt{2}} & 0 \\ 0 & -\frac{\lambda}{\sqrt{2}} & -k^+\gamma_1 & 0 & 0 & 0 & 0 & \frac{\lambda}{2} & 0 & \frac{i\lambda}{\sqrt{2}} \\ i\lambda & 0 & 0 & 0 & 0 & 0 & -\frac{i\lambda}{\sqrt{2}} & 0 & 0 & 0 \\ 0 & -i\lambda & 0 & 0 & 0 & 0 & 0 & -\frac{i\lambda}{\sqrt{2}} & 0 & 0 \end{pmatrix}, \tag{27}$$

which is correct to $O(k)$. Here, $k^+ \equiv \sqrt{2}(k_y + ik_x)$, $k^- \equiv \sqrt{2}(k_y - ik_x)$, and, for simplicity, we have retained only the V_σ TB hopping term and γ_1 electric-field term (taking $\gamma_2 = \gamma_3 = 0$. More complete expressions are derived in Table II). Within each 2D subspace, the effect of the remaining eight orbitals may be taken into account via the Löwdin downfolding [29].

The Löwdin downfolding works by partitioning the Hamiltonian in the secular equation $(H - EI)|\psi\rangle = 0$ into blocks,

$$H = \begin{pmatrix} h & b \\ b^\dagger & c \end{pmatrix}, \tag{28}$$

where the two blocks are well separated in energy. The effective Hamiltonian in the subspace h can be written as

$$h' = h + b(EI - c)^{-1}b^\dagger, \tag{29}$$

which, however, involves the eigenvalue E of the full Hamiltonian and needs to be solved iteratively. In the limit that the states in h and c are well separated and the coupling b is small, we can substitute E by the eigenvalues of matrix h. Also, it can be shown that an iterative solution of Eq. (29) produces Brillouin-Wigner perturbation series, which to the lowest order

yields

$$h'_{ij} = h_{ij} + \sum_k \frac{b_{ik} b^*_{kj}}{E - c_{kk}}. \tag{30}$$

If $|b_{ik}| \ll |h_{ii} - c_{kk}|$, the eigenvalues E can be replaced by the diagonal elements h_{ii}. Following this procedure, the effective Hamiltonian within each 2D subspace can be obtained. For example, for the Γ''_6 state, we get

$$\mathcal{H}_R = \begin{pmatrix} \varepsilon & \alpha_R(k_y + ik_x) \\ \alpha_R(k_y - ik_x) & \varepsilon \end{pmatrix}, \tag{31}$$

which can be written in the Rashba form $\mathcal{H}_R = \varepsilon + \alpha_R(k_y\sigma_x - k_x\sigma_y)$, with $\varepsilon = -\lambda/2$ and the Rashba coefficient $\alpha_R = -2\sqrt{3}\lambda\gamma_1/V_\sigma$ from Eq. (27). Complete expressions for all states are given in Table. II.

We see that both the spin-orbit coupling and the electric field are necessary to produce the Rashba term. Note that σ represents *not* the real spin, but rather the spin-orbital entangled pseudospin, which for the present example of the Γ''_6 case as seen from Eq. (26) is

$$\begin{aligned} |\uparrow\rangle &\equiv \frac{1}{\sqrt{2}}(d_{xz\downarrow} + id_{yz\downarrow}), \\ |\downarrow\rangle &\equiv \frac{1}{\sqrt{2}}(d_{xz\uparrow} - id_{yz\uparrow}). \end{aligned} \tag{32}$$

Finally, here we assumed that the field-induced parameters are smaller than spin-orbit coupling, i.e., $\gamma_i \ll \lambda$. However, if they are comparable, the off-diagonal elements in the subspace of Γ''_6,Γ''_7 become as strong as the on-site terms and the downfolding method breaks down. In such cases, one must either use degenerate perturbation theory to change the basis such that the off-diagonal matrix elements vanish or work with the full 4×4 Hamiltonian in the combined subspace [6].

B. Strong SOI ($\lambda \gg V$)

For the opposite limit, when spin-orbit is much stronger, the energy levels are shown in Fig. 6(b). The angular momentum states $j = 5/2$ and $3/2$ with energies λ and $-3\lambda/2$ split further due to the electron hopping. The characters of the bands are approximately the eigenfunctions of the spin-orbit Hamiltonian $H_{\rm SO}$, which preserve the symmetry of the lattice,

$$\begin{aligned}
\Gamma'_7 &= \begin{cases} \frac{1}{\sqrt{10}}(2d_{x^2-y^2\uparrow} - 2id_{xy\uparrow} - d_{xz\downarrow} + id_{yz\downarrow}) \\ \frac{1}{\sqrt{10}}(2d_{x^2-y^2\downarrow} + 2id_{xy\downarrow} + d_{xz\uparrow} + id_{yz\uparrow}), \end{cases} \\
\Gamma''_7 &= \begin{cases} \frac{1}{\sqrt{15}}(3id_{x^2-y^2\uparrow} - 2d_{xy\uparrow} + id_{xz\downarrow} + d_{yz\downarrow}) \\ \frac{1}{\sqrt{15}}(3id_{x^2-y^2\downarrow} + 2d_{xy\downarrow} - id_{xz\uparrow} + d_{yz\uparrow}), \end{cases} \\
\Gamma'''_7 &= \begin{cases} \frac{1}{\sqrt{3}}(d_{xy\uparrow} + id_{xz\downarrow} + d_{yz\downarrow}) \\ \frac{1}{\sqrt{3}}(-d_{xy\downarrow} - id_{xz\uparrow} + d_{yz\uparrow}), \end{cases} \\
\Gamma'_6 &= \begin{cases} \frac{1}{\sqrt{10}}(2d_{z^2\uparrow} + \sqrt{3}d_{xz\downarrow} + \sqrt{3}id_{yz\downarrow}) \\ \frac{1}{\sqrt{10}}(2d_{z^2\downarrow} - \sqrt{3}d_{xz\uparrow} + \sqrt{3}id_{yz\uparrow}), \end{cases} \\
\Gamma''_6 &= \begin{cases} \frac{1}{\sqrt{5}}(\sqrt{3}d_{z^2\uparrow} - d_{xz\downarrow} - id_{yz\downarrow}) \\ \frac{1}{\sqrt{5}}(\sqrt{3}d_{z^2\downarrow} + d_{xz\uparrow} - id_{yz\uparrow}). \end{cases}
\end{aligned} \tag{33}$$

In this basis, the spin-orbit part of the Hamiltonian is diagonal. But, since the basis set is spin mixed, the electric field now has off-diagonal matrix elements within each 2D subspace. This is unlike the weak SOI case, where the basis set was spin pure [see Eq. (26)], and therefore the electric field did not contain an off-diagonal term within each 2D subspace. Taking the example of the Γ'_6 doublet, we find the 2×2 TB matrix within this subspace has the same form as Eq. (31) with $\varepsilon = -3\lambda/2 + (2V_\sigma + 6V_\pi)/5$ and, again, the matrix has the Rashba form with $\alpha_R = -4\sqrt{3}\gamma_1/5$. The Löwdin downfolding that takes into account the effects of the other eight orbitals will produce higher-order terms $O(\gamma/\lambda)$ or $O(\gamma/V)$ because of the energy denominator. These terms are small compared to the leading terms listed in Table II because the electric field is assumed to be small leading to $\gamma \to 0$.

V. COMPARISON WITH DFT

To gauge the accuracy of our model, we compare the results with that of first-principles calculations using DFT. The simulation cell is as shown in Fig. 2. The weak and strong SOI cases are simulated using Ti and Ta atoms. The DFT calculations were carried out using the Vienna *ab initio* simulation package (VASP) [30], within the projector augmented wave method. We used the local density approximation including the spin-orbit interactions with a plane-wave energy cutoff of 350 eV and k-space sampling on a $9 \times 9 \times 1$ Monkhorst-Pack grid. We considered a single layer of atoms (Ti or Ta) on a square lattice, shown in Fig. 2. The unit cell was 10 Å long along the c axis, so that the large vacuum layer avoids any interaction with periodic images. The effect of the electric field is added via a sawtoothlike potential and using dipole corrections to help the energy convergence.

The parameters used in the calculations are given in Table III and the resulting band structures for the two cases are shown in Fig. 7. The bands are plotted along $k_{||}$ which lie in the xy plane around the Γ point. The TB parameters in Table III are chosen such that there is good agreement between the DFT and TB bands, as seen from Fig. 7. The Rashba coefficients are obtained from the slope of the Rashba band splitting $\Delta_R = 2\alpha_R k_{||}$, as shown in Fig. 8(b). The results are shown in Table II. The numerical values obtained from the TB expressions more

TABLE III. Parameters used in the DFT and TB calculations for the two cases, viz., weak and strong spin-orbit interaction. The lattice constants in DFT are chosen such that the d bands are well separated from the other bands and the TB parameters have been obtained by fitting to the DFT bands.

	DFT	TB fitting parameters
Weak SOI	Atom: Ti $a = b = 4$ Å $c = 10$ Å $E = 0.5$ eV/Å	$V_\sigma = -0.17$ eV, $V_\pi = 0.07$ eV, $V_\delta = -0.02$ eV, $\lambda = 0.02$ eV, $\gamma_1 = 25$ meV, $\gamma_2 = 10$ meV, $\gamma_3 = 2$ meV
Strong SOI	Atom: Ta $a = b = 5$ Å $c = 10$ Å $E = 0.5$ eV/Å	$V_\sigma = -0.1$ eV, $V_\pi = 0.05$ eV, $V_\delta = -0.01$ eV, $\lambda = 0.18$ eV, $\gamma_1 = 6.5$ meV, $\gamma_2 = 18$ meV $\gamma_3 = 1$ meV

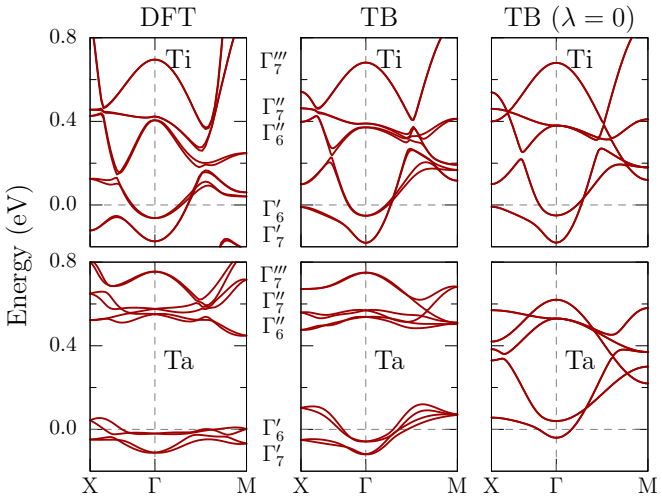

FIG. 7. (Color online) Comparison of the TB and DFT band structures for Ti and Ta, which show weak and strong SO coupling, respectively. Symmetries of the wave functions at the Γ point are shown between the plots. A small orbital-dependent on-site energy is added to the TB Hamiltonian to better fit the DFT bands, and the Fermi energy has been set to zero.

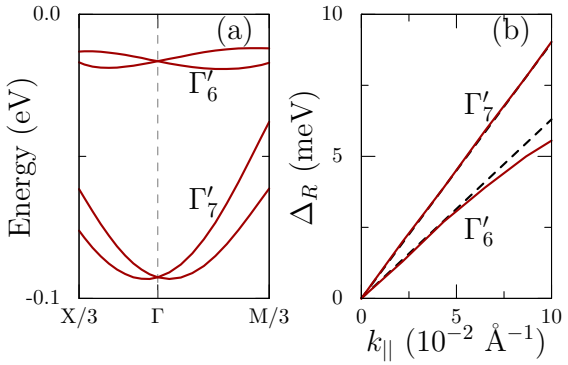

FIG. 8. (Color online) (a) A closer look at the lowest two DFT bands around the Γ point for Ta from Fig. 7 and (b) the Rashba band splitting $\Delta_R = 2\alpha_R k_{||}$, which shows the linear momentum dependence.

or less agree with the full calculations (TB or DFT); there are some disagreements in the magnitudes, however, because the weak and strong SOI limits ($\lambda \to 0$ or ∞) are not fully satisfied in the realistic systems. Nevertheless, it is clear that the Rashba coefficients are quite strongly orbital dependent.

VI. SUMMARY

In summary, we studied the Rashba effect in the *d* electron systems and showed that the effect depends strongly on the orbitals involved in a particular band. This was illustrated by density functional studies for selected systems in the limit of both weak and strong SOI. The symmetry-breaking electric field introduces matrix elements in two distinct ways, viz., via mixing of the atomic orbitals on the same site and by introducing intersite hopping terms within the tight-binding description, both of which we examined in studying the Rashba effect. Using the tight-binding model, we derived the expressions for the Rashba coefficients in both limits of weak and strong SOI. The *d* electron systems offer a rich system for manipulating the Rashba effect, not only because the magnitude of the effect can be strong owing to the large atomic numbers *Z*, but also because the orbital characters and the band energies are sensitive to external forces such as strain, which can be used for tailoring the effect for potential applications in oxide electronics.

ACKNOWLEDGMENTS

This research was supported by the US Department of Energy, Office of Basic Energy Sciences, Division of Materials Sciences and Engineering under Award No. DE-FG02-00ER45818.

[1] E. I. Rashba, Sov. Phys. Solid. State **2**, 1109 (1960).
[2] A. D. Caviglia, M. Gabay, S. Gariglio, N. Reyren, C. Cancellieri, and J.-M. Triscone, Phys. Rev. Lett. **104**, 126803 (2010).
[3] S. Datta and B. Das, Appl. Phys. Lett. **56**, 665 (1990).
[4] Y. A. Bychkov and E. I. Rashba, J. Phys. C **17**, 6039 (1984).
[5] G. Bihlmayer, Y. Koroteev, P. Echenique, E. Chulkov, and S. Blügel, Surf. Sci. **600**, 3888 (2006).
[6] K. V. Shanavas and S. Satpathy, Phys. Rev. Lett. **112**, 086802 (2014) Note: Equation (1) of this paper has a minus sign error. The correct sign convention followed throughout that paper as well as the current paper is given by the expression for the Rashba effect, viz., $\mathcal{H}_R = \alpha_R(\vec{\sigma} \times \vec{k}) \cdot \hat{z}$.
[7] S. LaShell, B. A. McDougall, and E. Jensen, Phys. Rev. Lett. **77**, 3419 (1996).
[8] Y. M. Koroteev, G. Bihlmayer, J. E. Gayone, E. V. Chulkov, S. Blügel, P. M. Echenique, and P. Hofmann, Phys. Rev. Lett. **93**, 046403 (2004).
[9] K. Ishizaka, M. S. Bahramy, H. Murakawa, M. Sakano, T. Shimojima, T. Sonobe, K. Koizumi, S. Shin, H. Miyahara, A. Kimura, K. Miyamoto, T. Okuda, H. Namatame, M. Taniguchi, R. Arita, N. Nagaosa, K. Kobayashi, Y. Murakami, R. Kumai, Y. Kaneko, Y. Onose, and Y. Tokura, Nat. Mater. **10**, 521 (2011).
[10] P. D. C. King, R. C. Hatch, M. Bianchi, R. Ovsyannikov, C. Lupulescu, G. Landolt, B. Slomski, J. H. Dil, D. Guan, J. L. Mi, E. D. L. Rienks, J. Fink, A. Lindblad, S. Svensson, S. Bao, G. Balakrishnan, B. B. Iversen, J. Osterwalder, W. Eberhardt, F. Baumberger, and P. Hofmann, Phys. Rev. Lett. **107**, 096802 (2011).
[11] M. Ben Shalom, M. Sachs, D. Rakhmilevitch, A. Palevski, and Y. Dagan, Phys. Rev. Lett. **104**, 126802 (2010).
[12] H. Nakamura, T. Koga, and T. Kimura, Phys. Rev. Lett. **108**, 206601 (2012).

[13] P. D. C. King, R. H. He, T. Eknapakul, P. Buaphet, S.-K. Mo, Y. Kaneko, S. Harashima, Y. Hikita, M. S. Bahramy, C. Bell, Z. Hussain, Y. Tokura, Z.-X. Shen, H. Y. Hwang, F. Baumberger, and W. Meevasana, Phys. Rev. Lett. **108**, 117602 (2012).
[14] L. Petersen and P. Hedegård, Surf. Sci. **459**, 49 (2000).
[15] T. Kosugi, T. Miyake, and S. Ishibashi, J. Phys. Soc. Jpn. **80**, 074713 (2011).
[16] C. L. Kane and E. J. Mele, Phys. Rev. Lett. **95**, 226801 (2005).
[17] S. Konschuh, M. Gmitra, and J. Fabian, Phys. Rev. B **82**, 245412 (2010).
[18] C. R. Ast and I. Gierz, Phys. Rev. B **86**, 085105 (2012).
[19] Z. Zhong, A. Tóth, and K. Held, Phys. Rev. B **87**, 161102 (2013).
[20] G. Khalsa, B. Lee, and A. H. MacDonald, Phys. Rev. B **88**, 041302 (2013).
[21] Y. Kim, R. M. Lutchyn, and C. Nayak, Phys. Rev. B **87**, 245121 (2013).
[22] L. D. Landau and L. M. Lifshitz, *Quantum Mechanics: Non-relativistic Theory* (Butterworth-Heinemann, Oxford, 1991).
[23] E. U. Condon and G. H. Shortley, *The Theory of Atomic Spectra* (Cambridge University Press, Cambridge, 1935).
[24] F. Herman and S. Skillman, *Atomic Structure Calculations* (Prentice-Hall, New Jersey, 1963).
[25] J. C. Slater and G. F. Koster, Phys. Rev. **94**, 1498 (1954).
[26] W. A. Harrison, *Electronic Structure and the Properties of Solids: The Physics of the Chemical Bond* (Freeman, San Francisco, 1980).
[27] H. L. Skriver, *The LMTO Method: Muffin-Tin Orbitals and Electronic Structure* (Springer, Verlag, 2011).
[28] J. A. Gaunt, Philos. Trans. R. Soc. A **228**, 151 (1929).
[29] P.-O. Löwdin, J. Chem. Phys. **19**, 1396 (1951).
[30] G. Kresse and J. Hafner, Phys. Rev. B **47**, 558 (1993).